npj | space exploration

Article

https://doi.org/10.1038/s44453-026-00027-y

Impact-induced high-temperature formation of metallic copper and bornite in Chang'e-6 lunar soils

Zhuang Guo[1] ✉, Dongsheng Song[2], Wenlei Song[1], Chen Li[3], Ronghua Pang[3], Yuqi Qian[4], Kangjun Huang[1], Yang Li[3] ✉ & Guochun Zhao[1,4]

Impacts play a critical role in modifying the chemical and structural characteristics of materials and in facilitating the migration of moderately volatile elements on airless bodies. In this study, a comprehensive SEM–FIB–TEM analysis of a Cu-rich grain from the recently returned Chang'e-6 lunar soil demonstrates that an assemblage of metallic copper, metallic iron, and Fe^{3+}–Cu sulfides (i.e., bornite, Cu_5FeS_4) was formed under impact-induced high-temperature conditions. This finding provides evidence for the presence of bornite in lunar soils. The relatively homogeneous distribution of bornite, confined to the topmost surface of the Cu-rich grain coating, indicates a vapor-deposition origin. According to the thermodynamic modeling, the observed assemblages of metallic copper, metallic iron, and FeS within the grain interior can be explained by equilibrium thermodynamic behavior of the Cu–Fe–S system at elevated temperatures. The complex mineralogy involving Fe^{3+}-bearing bornite, metallic iron, and metallic copper in the lunar soil further indicates that impact-induced melting and vaporization processes substantially perturb the valence states of metallic elements in the Cu–Fe–S system, thereby enabling the generation and stabilization of metallic phases and oxidized copper sulfides in lunar materials. Such natural high-temperature metallurgical processes provide critical insights into understanding extraterrestrial metal migration and enrichment under impact conditions on airless bodies.

Investigating metallogenic processes in extraterrestrial environments is essential for advancing extraterrestrial resource utilization on airless bodies[1,2]. Impact processes play a critical role in reprocessing and modifying the chemical and microstructural properties of extraterrestrial materials and are regarded as a unique extraterrestrial ore-forming process on airless bodies. The airless Moon and asteroids share similar surface environments characterized by high vacuum, low gravity, and high impact flux[3], with lunar exploration missions (Apollo, Luna, and Chang'E) having returned a substantially larger number of samples than asteroid missions[4,5]. Accordingly, investigating the migration and redox behavior of metallic elements in lunar regolith provides fundamental insights into metal concentration mechanisms on airless bodies. Copper is a key industrial metal and provides long-term economic value. The Cu–Fe–S system is among the most important natural ternary sulfide systems and represents a major class of terrestrial ore-forming assemblages[6]. A detailed understanding of the chemical behavior of the Cu–Fe–S system under impact-induced high-temperature conditions on the surfaces of airless bodies can provide insights into natural beneficiation mechanisms that concentrate elemental copper on these bodies.

Copper species have been extensively documented in asteroid samples, with metallic copper reported in approximately 66% of ordinary chondrites, and Cu concentrations in these meteorites ranging between 68 and 85 ppm[7–10]. Cu-bearing materials have also been identified in samples returned from the asteroid Itokawa[11]. Whereas Cu-bearing materials have been rarely reported in lunar samples, reported copper species in lunar materials include native copper[12–15], vapor-deposited digenite[16,17], and igneous Cu-Fe-S phases (e.g., chalcopyrite, cubanite)[12,18,19]. During the Apollo era, analyses of copper materials in lunar samples were primarily semiquantitative, with limited structural data[13]. More recently, detailed microscopic studies of Chang'e-5 samples have documented the presence of native copper and digenite on the Moon, concentrated on grain surfaces and

[1]Department of Geology, State Key Laboratory of Continental Evolution and Early Life, NWU-HKU Joint Center of Earth and Planetary Sciences, Northwest University, Xi'an, China. [2]Institutes of Physical Science and Information Technology, Anhui University, Hefei, China. [3]Center for Lunar and Planetary Sciences, Institute of Geochemistry, Chinese Academy of Sciences, Guiyang, China. [4]Department of Earth Sciences & NWU-HKU Joint Center of Earth and Planetary Sciences, The University of Hong Kong, Hong Kong, China. ✉e-mail: guozhuang@nwu.edu.cn; liyang@mail.gyig.ac.cn

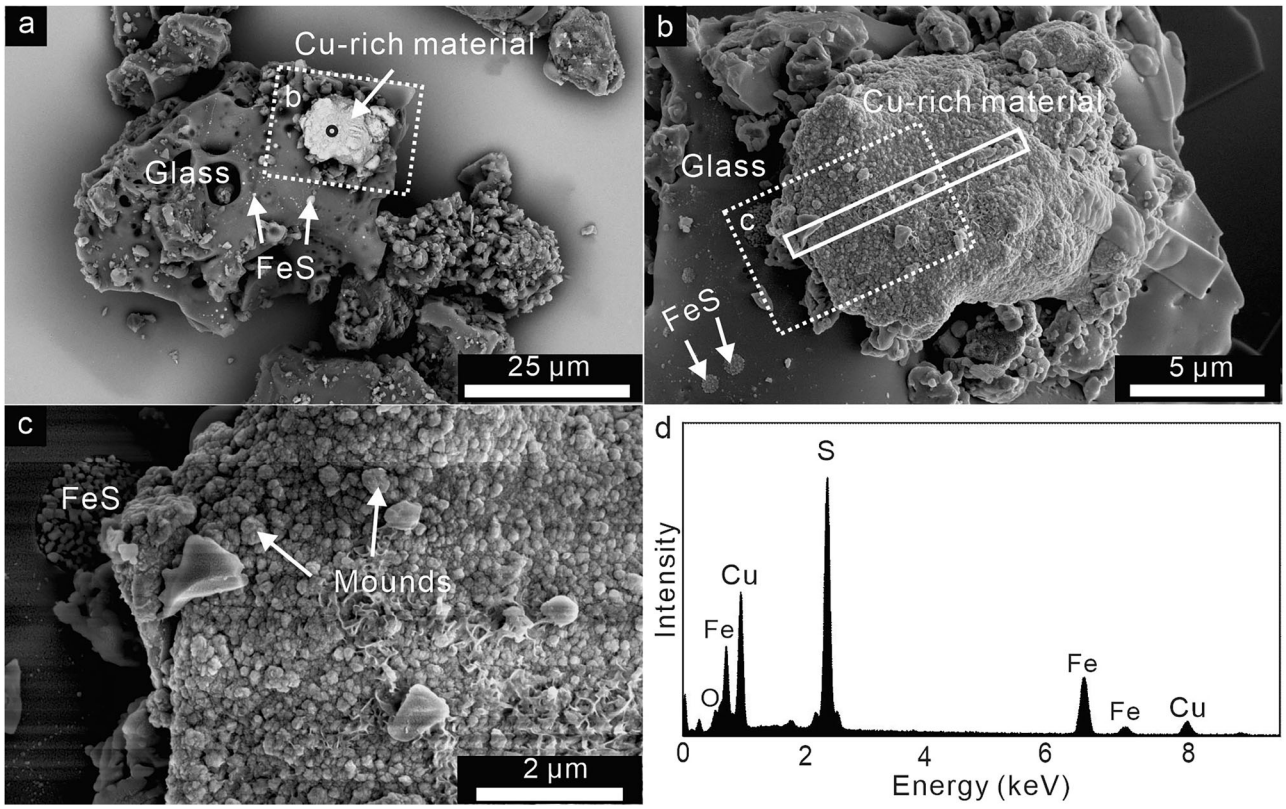

Fig. 1 | Overview of the Cu-rich grain in Chang'e-6 lunar soil. a Back-scattered electron (BSE) image of the Cu-rich grain embedded in a glassy agglutinate of Chang'e-6 lunar soil. **b** Secondary electron (SE) micrograph observations of the Cu-rich grain. The solid rectangle represents the location of the FIB slice extraction. **c** A close-up SE image of the morphology of the Cu-rich material surface. **d** SEM-EDS spectra of the Cu-rich material.

interpreted to be associated with impact-induced vapor-deposition processes[16,17].

China's Chang'e-6 mission successfully landed in the Apollo impact crater within the South Pole–Aitken basin, the largest lunar impact basin, and returned a total of 1935.3 g of lunar samples[20–23]. The geological context of the Chang'e-6 landing site and analyses of the returned samples indicate extensive impact-driven modification of lunar soils[22,24,25]. In this study, a detailed SEM–FIB–TEM investigation was conducted on a Cu-rich grain from Chang'e-6 lunar soils that had undergone impact modification. The assemblage of metallic copper, metallic iron, and bornite (Cu_5FeS_4) was identified within the Cu-rich grain, which was formed through impact-induced melting and evaporation processes. The occurrence of this copper-species assemblage is consistent with stability fields defined by the Cu–Fe–S phase diagram under high-temperature conditions, thereby reflecting complex redox transitions and elemental migration within the Cu–Fe–S system during impact-induced high-temperature processes on airless bodies.

Results

The Chang'e-6 returned lunar samples contain a high proportion of glassy materials (27.9 vol.%), most of which originated from impact processes and occur within agglutinates and breccia clasts[24]. One Cu-rich grain (~15 μm in diameter) was identified among tens of thousands of fine-grained Chang'e-6 lunar soils examined by SEM-based automated mineralogy (TESCAN Integrated Mineral Analyzer, TIMA) method, highlighting the rarity of Cu-bearing grains in Chang'e-6 lunar samples (Supplementary Fig. 1). Back-scattered electron (BSE) imagery shows that the Cu-rich grain, with the brightest contrast, is located on a ~ 50 μm glassy agglutinate particle, and the grain exhibits Cu-, Fe-, and S-rich compositional features in the SEM-EDX elemental maps (Fig. 1). A large number of microscopic rounded iron-sulfide grains are observed embedded within the agglutinate glass (Fig. 1a), and such morphological features of iron-sulfide (FeS) have been described as "hemispherical mounds" in previous studies and are interpreted as impact-related products[26,27]. Close-up secondary electron (SE) images show that the surface of the Cu-rich grain is coated with uniform, nanoscale mounds, which are consistent with the characteristics of previously reported copper-rich materials deposited on the surfaces of Chang'e-5 lunar soil (Fig. 1b)[16,17]. The EDX spectra of the Cu-rich material indicate it is dominated by elemental Fe, S, and Cu and lacks detectable Ni or Co (Fig. 1d). This composition is distinct from that of metallic copper occurring in Fe(Ni)–troilite assemblages in ordinary chondrites, which typically contain elevated nickel contents[7,9].

Microscopic characteristics of the Cu-rich grain

An FIB cross-section was prepared to characterize the mineral chemistry and crystallography of the Cu-rich material in detail. TEM analysis shows that the mineral assemblage within the FIB cross-section consists of Cu–Fe–S grain coexisting with a large pure metallic iron particle (Fe^0, approximately 5 μm in diameter) and apatite (Fig. 2a, Supplementary Fig. 2, and Fig. 3). The large Fe^0 particle (located in the lower-left corner of Fig. 2a) exhibits a curved grain boundary, suggesting that it experienced localized grain-boundary melting, consistent with features of partial melting reported in meteorites[28]. Moreover, veins of iron sulfide were observed intruding into the interior of apatite, which is attributed to shock-induced melting of iron sulfide due to its lower melting point (<1000 °C) relative to apatite (Fig. 2b). The crystal structures of the iron sulfide, large Fe^0, and apatite grains were further determined based on Selected area electron diffraction (SAED) patterns (Fig. 2c–e).

TEM images indicate that the Cu-Fe-S grain is composed of three distinct zones: a surface coating Fe–Cu sulfide layer (~200 nm in thickness), a Cu^0-free zone, and a Cu^0-rich zone containing numerous submicron-sized inclusions (Fig. 2b and Supplementary Fig. 3). TEM-EDX spectra and

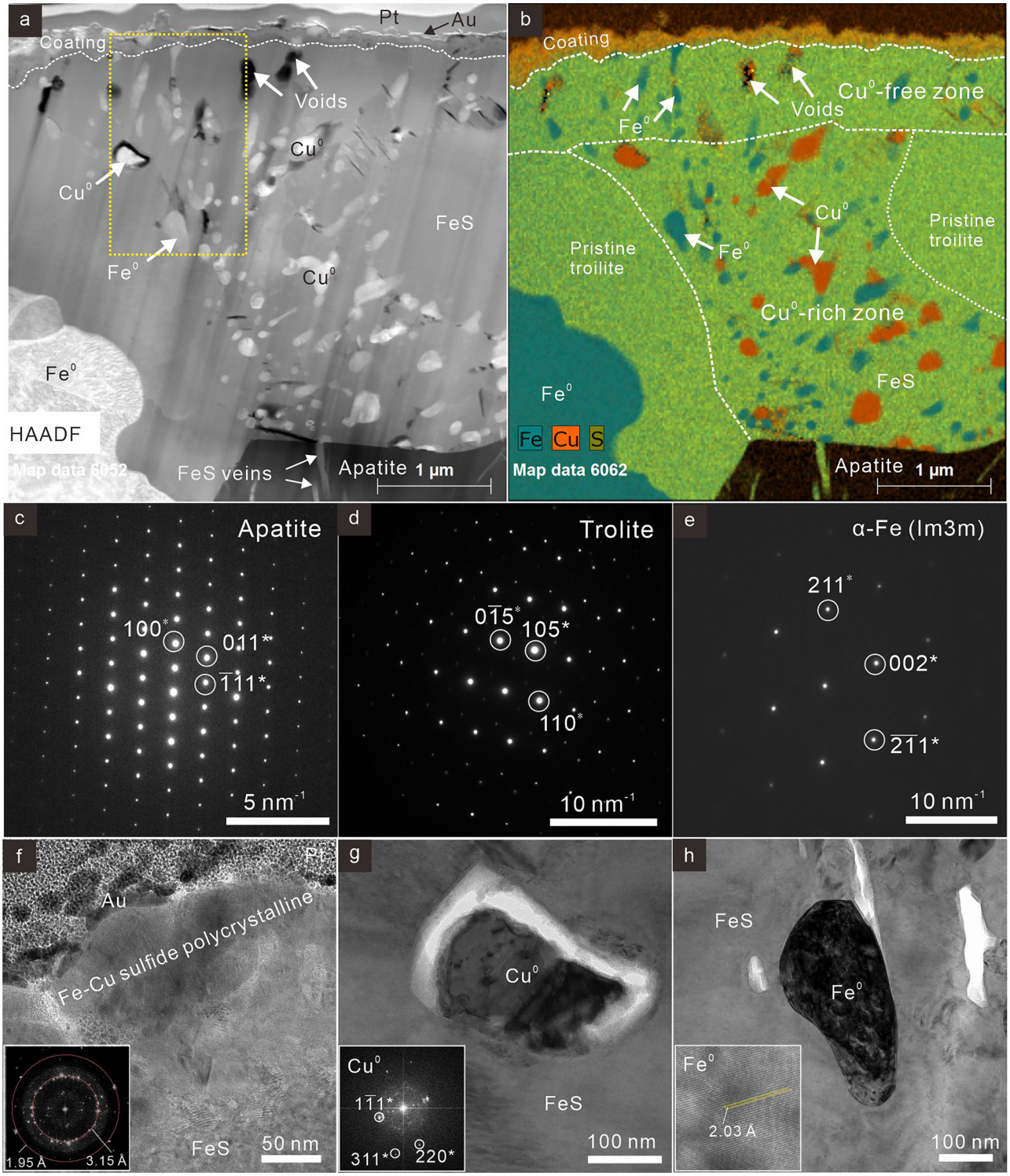

Fig. 2 | Microstructure and chemical characteristics of the interior of the Chang'e-6 Cu-rich grain. a, **b** High-angle annular dark-field (HAADF) image of the FIB slice and corresponding quantitative TEM-EDX element maps of Cu, S, and Fe. The yellow dashed rectangle represents the region of the EELS maps in Fig. 3. **c–e** Selected area electron diffraction pattern of the apatite, troilite, and Fe^0 particles in the FIB section. **f–h** TEM bright-field image and high-resolution TEM (HRTEM) images of the deposited Fe-Cu-sulfide layer, metallic copper, and metallic iron. The fast Fourier transform (FFT) patterns and lattice fringe of these phases are inserted in the lower-left of the images.

compositional maps indicate that the surface coating is dominated by Cu–Fe–S components, with no detectable silicate elements (e.g., Si, Mg, Al, or Ca) (Fig. 2b and Supplementary Fig. 3). Fast Fourier transform patterns derived from high-resolution TEM (HRTEM) images of the coating phases exhibit a diffraction ring, indicating that the coating is characterized by nanosized polycrystalline structures (Fig. 2f). Although the Cu–K peak in EDS spectra is significantly influenced by Cu from the FIB grid, the Cu–L peak predominantly reflects Cu present within the analyzed sample, and spectra obtained from Fe^0 and troilite phases show no detectable Cu–L signal (Supplementary Fig. 4). EDS spectra obtained from the Cu–Fe sulfide coating indicate that the Cu–L peak intensity is significantly higher than that of Fe, and EDS semiquantitative analyses reveal a high Cu abundance

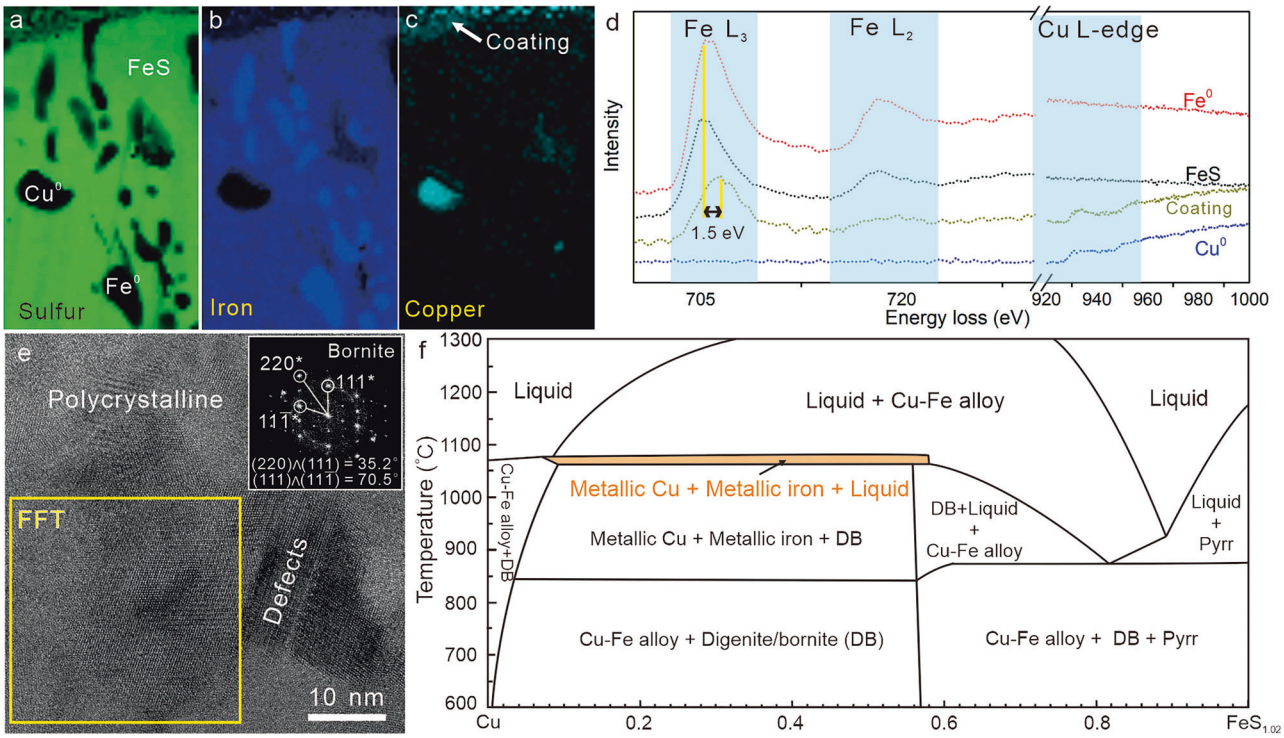

Fig. 3 | EELS spectra and crystal structure of metallic copper and bornite. **a**–**c** EELS elemental maps of S, Fe, and Cu for the Cu-rich material in the FIB section. **d** EELS spectrum images (SI) of the main phases within the Cu-rich material, including Fe^0 and Cu^0 inclusions, FeS, and the Fe-Cu sulfide coating. **e** HRTEM image of the Fe–Cu sulfide coating, with the corresponding FFT pattern inserted in the upper-right corner and indexed to bornite. **f** Cu–Fe–S phase diagram adapted from Waldner (2025). Pyrr refers to pyrrhotite.

Table 1 | Quantitative TEM–EDS analyses of the phases in the FIB section

Phases	Fe (at%)	Cu (at%)	S (at%)	(Fe + Cu)/S
Coating	16.8	55.3	27.9	2.58
Cu^0-free zone matrix	47.2	9.85	43.0	1.33
Cu^0-rich zone matrix	42.24	14.80	43.0	1.33
Pristine troilite	49.52	10.67	39.81	1.51
Metallic copper	1.84	96.6	1.57	
Metallic iron	86.0	11.5	2.46	

The TEM–EDS data have been normalized to 100%. The detectable Cu present in the metallic iron and pristine troilite is interpreted to result from contamination by the Cu support grid during the EDS analyses.

(Supplementary Fig. 4, Table 1). EELS mapping results further confirm that the coating phase consists of Fe, S, and Cu, with a significantly stronger signal observed for Cu than for Fe (Fig. 3). In addition, a distinct EELS Fe-L_3 peak shift toward higher energy losses of approximately 1.5 eV relative to those of Fe^{2+}/Fe^0 was detected in the Cu–Fe sulfide polycrystalline coating (Fig. 3d), indicating that the valence state of iron in the Cu–Fe sulfide coating is dominated by Fe^{3+}. The quantitative EDS and EELS data for the coating are consistent with the stoichiometric composition of bornite (Cu_5FeS_4).

SAED patterns obtained from the coating exhibit the most intense diffraction reflections at ~1.9 and ~3.2 Å, and HRTEM images of the polycrystalline coating can be partially indexed to mineral bornite (Cu_5FeS_4) with a high density of crystallographic defects (Figs. 2f, 3e), rather than to chalcopyrite or digenite previously reported in lunar samples. Notably, the Cu–Fe sulfide coating contains additional nanocrystalline phases, as evidenced by extra diffraction spots in Fig. 3e, which cannot be conclusively indexed based on the current chemical and crystallographic data. Based on these detailed chemical and structural observations, the surface coating on the Cu–Fe–S grain is dominated by Fe^{3+}-Cu sulfide occurring in a polycrystalline form, with bornite identified as the primary phase.

The Cu^0-free zone occurs as an intermediate layer between the coating and the Cu^0-rich zone, characterized by the exclusive presence of elongate metallic iron inclusions (~100 nm in length) and vesicles, with Cu content lower than that of both the coating and the Cu^0-rich zone (Fig. 2b; Table 1). In contrast, the Cu^0-rich zone contains abundant submicroscopic inclusions with grain sizes of approximately 80–300 nm, exhibiting pronounced enrichment in elemental iron or copper (Fig. 2; Table 1). TEM bright-field images show that the crystallographic orientation of the inclusion-rich region is distinct from that of the pristine troilite grain (Supplementary Fig. 3d), and both the Cu^0-free and Cu^0-rich zones exhibit sulfur-deficient compositions, with bulk atomic (Cu + Fe)/S > 1 (Fig. 2b, Table 1). The EELS spectra of the pure elemental iron particles within the Cu^0-rich zone exhibit strong Fe L-edge peaks, with no detectable Cu or S signals (Fig. 3d). The pure copper particles exhibited only a signal from the Cu EELS L-edge (Fig. 3d). Additionally, HRTEM images further confirm the identification of the pure iron phase as metallic α-Fe and the pure copper phase as metallic Cu (Fig. 2g and h). Collectively, the inclusions embedded within the Cu^0-rich zone were confirmed to be metallic iron and metallic copper. EELS and TEM–EDS mapping also show that oxygen is spatially associated with voids rather than being consistently co-located with copper-rich regions in the grain interior (Supplementary Figs. 3f and 5b), suggesting that the oxygen surrounding the voids in the FIB foil most likely originates from terrestrial oxidation during sample preparation.

Discussion

Copper, a resource of significant industrial and economic value, is commonly found in extraterrestrial samples as metallic copper (native Cu or Cu alloys) and sulfide minerals (e.g., chalcopyrite, cubanite, and bornite)[7,9,10,19].

Previous studies have shown that troilite commonly intergrows with native iron in Apollo igneous rocks, and cupriferous sulfides may form as an exsolution product from troilite during the crystallization of immiscible Cu-bearing sulfide liquids[19]. Additionally, endogenous metallic iron grains in lunar mare basalts are typically submicron- to micron-sized and exhibit low nickel contents (<1 wt%)[15,18,19,29]. In the studied Cu-rich grain from the Chang'e-6 sample, a large native Fe^0 particle (~5 μm) is observed to coexist with sulfide phases (Fig. S2a), and no detectable Ni or Co signals are identified in any phase (Supplementary Fig. 4). Notably, apatite—widely recognized as an accessory mineral that crystallizes during the late stages of igneous differentiation—is entirely enclosed within the sulfide phase (Supplementary Fig. 2). This spatial association strongly supports an endogenous lunar igneous origin for the apatite–Fe^0–cupriferous sulfide assemblage of the Cu-rich grain, rather than derivation from primitive meteoritic contamination[9,11,15]. The features of partially melting of large Fe^0 particle, the presence of sulfide veins intruding into the apatite, and the recrystallization of troilite, indicate that the studied Cu-rich grain experienced impact-induced partial melting of an Fe^0–sulfide assemblage at a temperature of approximately 988 °C[6,30].

Within the Cu^0-rich zone, the coexistence of metallic Cu and metallic Fe was observed, characterized by a pronounced sulfur-deficient composition, and these metallic inclusions are distinct from previously reported nanophase iron particles ($npFe^0$), wire-like metallic Cu, or Cu-rich deposits on the uppermost surfaces of lunar grains in Apollo and Chang'e-5 samples[12,17]. The observations suggest that the metallic iron and metallic copper embedded within the Cu^0-rich zone of the Chang'e-6 Cu-rich grain have a melt-derived origin, rather than forming through vapor deposition processes. Experimental studies of the Cu–Fe–S system under high-temperature melting conditions have demonstrated extensive liquid immiscibility, leading to the segregation of Cu-rich sulfide melts at elevated temperatures[6]. Thermodynamic modeling based on Gibbs energy minimization further indicates that both metallic Cu and metallic Fe remain stable over a wide compositional range in the Cu–Fe–S system at high temperatures[31,32]. Textural evidence, including sulfide veins intruding into apatite and recrystallization within inclusion-rich regions (Supplementary Fig. 3d), suggests that the Fe–S phase in the Cu^0-rich zone experienced partial melting. The coexistence of metallic Cu, metallic Fe, and Fe–S phases in equilibrium had been predicted as high-temperature stability fields in Cu-Fe-S system (Fig. 3f). According to the Cu–Fe–S phase diagram and experimental results, metallic iron and metallic copper are expected to be stable when the precursor composition has an atomic (Cu + Fe)/S ratio greater than 1 and undergoes high-temperature processing at approximately 1100 °C[6,31]. Therefore, the assemblage of metallic Cu, metallic Fe, and Fe–S phases observed in the Cu^0-rich zone is best interpreted as the equilibrium product of high-temperature melting of the Cu–Fe–S system under sulfur-deficient conditions.

In the studied Cu-rich grain, the surficial Cu^0-free zone is mineralogically and chemically distinct from the underlying Cu^0-rich zone. The Cu^0-free zone occurs as an intermediate layer between the surface coating and the Cu^0-rich zone and is characterized by the exclusive presence of metallic Fe and abundant vesicles within a Fe–S phase, with a Cu content markedly lower than that of both the adjacent coating and the Cu^0-rich zone. Thermodynamic calculations and in situ heating simulation experiments indicate that troilite readily undergoes desulfurization under high-temperature and vacuum conditions. Degassing processes are significantly enhanced at lunar troilite grain surfaces, and the reaction FeS = 2Fe + S2(g) can be activated at temperatures exceeding ~840 K under high-vacuum conditions (~10^{-9} Pa)[16,33]. The coexistence of pure metallic Fe and vesicular textures within the Cu^0-free zone therefore suggests thermal desulfurization of troilite. Accordingly, the Cu^0-free zone is interpreted to have formed through vacuum-induced thermal desulfurization during high-temperature exposure at the lunar surface, resulting in the development of vesicles and metallic Fe. The occurrence of the sulfide coating is inferred to have occurred after degassing of the Cu^0-free zone, which likely inhibited the formation of large volumes of metallic iron (e.g., iron whiskers) and extensive vesicular textures commonly observed on space-weathered troilite surfaces[33–37].

In addition to metallic copper, a Fe^{3+}–Cu sulfide coating layer (i.e., bornite), approximately 200 nm thick, was observed on the outermost surface of the Cu-rich grain. Similar "tiny dot" and mound-shaped morphologies have previously been used to describe vapor-deposited copper species on lunar soil surfaces[16,17]. The coating exhibits a mound-shaped morphology, a relatively uniform thickness, and a chemical composition distinct from that of the underlying troilite substrate, consistent with characteristics of vapor-deposited rims reported from Apollo and Chang'e-5 lunar soils[16,38,39]. Igneous Cu–Fe sulfide minerals (e.g., chalcopyrite and bornite) have been reported in lunar samples. These sulfides typically crystallize from immiscible sulfide liquids and commonly occur as eutectic intergrowths with metallic iron or Fe sulfides in lunar basalts[12]. The characteristics of the coating observed in this study are markedly different from those of igneous cupriferous sulfides with eutectic intergrowths, suggesting a distinct origin from endogenous bornite.

Vaporization is a ubiquitous process induced by impact events on airless bodies. Metallic nodules in ordinary chondrites, as well as $npFe^0$ and Fe–Si alloys in lunar samples, have been proposed to form through impact-induced vaporization and subsequent fractional condensation[12,40–42]. Vapor deposits commonly form on the outermost surfaces of lunar soils, and impact-induced vapor-deposited Cu phases, including native copper and digenite, have been previously identified in Apollo and Chang'e-5 lunar soils[12,16,17]. The surface coating on the studied Cu-rich grains exhibits a uniform lateral distribution, indicating that it most likely originates from vapor deposition. Both Cu and S behave as volatile elements under high-temperature and high-vacuum conditions, and Cu–S components exhibit relatively low vaporization temperatures (~840 K) under vacuum[16]. Previous investigations of lunar samples have demonstrated that Cu–S phases are readily vaporized and subsequently redeposited onto regolith grain surfaces[16,17]. The identification of bornite with a stoichiometric composition of Cu_5FeS_4 further indicates that Cu and S were the dominant constituents of the vapor phase, consistent with the preferential vaporization of Cu–S components.

According to the Cu–Fe–S phase diagram (Fig. 3f), bornite represents one of the most stable phases during the cooling of the Cu–Fe–S system at temperatures below ~1050 °C[6,31,43]. Therefore, the precursor of the deposited coating is interpreted to have been bornite, originally in equilibrium with metallic Fe and metallic Cu within the Cu^0-rich zone under high-temperature conditions. The same or a subsequent impact event likely triggered the vaporization of the bornite component from the Cu^0-rich zone, followed by the redeposition of the vaporized Cu–Fe sulfide onto the grain surface and the recrystallization of nano-sized bornite polycrystals.

In summary, the observed nanoscale metallic iron, metallic copper, and bornite are interpreted as products formed by high-temperature processing of the lunar immiscible Cu–Fe–S system, revealing the unique redox and compositional evolution pathways of the Cu–Fe–S system during impacts on the lunar surface. In addition to the impact-induced vapor deposition of Cu-bearing phases (e.g., native copper and digenite) previously reported in Chang'e-5 lunar soils[16,17], the behavior of elemental copper under molten conditions observed in the Chang'e-6 samples indicates that a more complex Cu–Fe–S mineral assemblage formed through high-temperature equilibration, in accordance with phase diagram predictions. Therefore, the high-temperature conditions induced by impact significantly regulate the migration and valence changes of metallic elements through melting and vapor condensation processes. Similar phenomena have also been confirmed in meteorite observations[9,40,42].

From both lunar samples and previous meteorite observations, elemental copper commonly coexists with metals and sulfides. Studies of melt veins in ordinary chondrites have shown that elemental Cu is preferentially incorporated into fine-grained Fe–Ni metal[7–10,12,13]. This supports the close association of elemental copper with sulfides and Fe metals, indicating that Fe metals and troilite serve as key carriers of copper in extraterrestrial materials. Our investigation further demonstrates that, under high-

temperature conditions, cupriferous sulfides can undergo complex mineralogical transformations and changes in elemental valence states, allowing copper to concentrate and form bornite and metallic copper on airless bodies. Such metal enrichment mechanisms, driven by external dynamic processes on airless bodies, are essential for advancing the in-situ utilization of extraterrestrial resources.

Methods

Samples

The studied Chang'e-6 lunar soil was a fine fraction sample of the surficial shoveled lunar regolith (CE6C0300YJFM and CE6C0500YJFM). The samples were dispersed onto a gold-plated one-inch silicon wafer using ≥99.8% high-purity ethanol. The ethanol was then evaporated using an infrared lamp to facilitate the adhesion of the fine lunar soil to the silicon wafer. The sample was subsequently coated with an additional gold film for scanning electron microscope (SEM) observations.

SEM and TESCAN Integrated Mineral Analyzer (TIMA) analysis

SEM-based automated mineralogy was employed in this study for the chemical characterization of a large number of fine lunar soils. This analysis was conducted using the TESCAN MIRA-3 SEM, which is equipped with four high-throughput EDAX silicon-drift EDS detectors, at the State Key Laboratory of Continental Dynamics, Northwest University. The analysis was conducted using the dot mapping acquisition mode with an EDS spacing of 3 μm. A total of 20,000 X-ray counts per EDS point was acquired to ensure high-quality elemental data. Measurements were conducted at an acceleration voltage of 25 kV, a beam current of 9 nA, and a working distance of 15 mm. In the prepared sample, more than 100,000 lunar soil particles were identified, and EDS elemental and phase mapping of these particles was also performed for analysis. The TIMA results show that one lunar soil grain exhibits copper enrichment, which is the main focus of this study (Supplementary Fig. 1). High-resolution secondary electron (SE) imaging, energy-dispersive X-ray spectroscopy (EDS) analysis, and focused ion beam (FIB) section preparation of the target lunar soil were performed using the Thermo Scientific Helios G4 UX DualBeam FIB-SEM at the Department of Geology, Northwest University. Due to the spectral overlap between Mo and S in EDS—which complicates the quantification of copper sulfide phases (S-Kα at 2.31 keV; Mo-Lα at 2.29 keV)—and considering that the porous nature of Mo grids increases the risk of sample loss during transfer, a copper grid was ultimately selected for FIB sample preparation.

Transmission electron microscopy (TEM) analysis

Chemical analyses of the FIB section, including TEM X-ray elemental mapping and EDS spectral acquisition, were carried out using the EDS detector on a Talos F200X scanning transmission electron microscope (STEM). Precise quantification of the TEM-EDS data was achieved through an interactive TEM quantitative method implemented in Bruker Esprit software. To minimize the potential influence of the copper grid on compositional analysis, the EDS Cu–L signal and electron energy loss spectroscopy (EELS) data were jointly utilized to differentiate grid-derived copper from copper present in the sample. High-resolution transmission electron microscopy (HRTEM) images and selected area electron diffraction (SAED) patterns were obtained to identify the mineral structures within the FIB section.

Electron energy-loss spectroscopy (EELS) analysis

The STEM-EELS experiments were conducted at 300 kV using a Thermo Fisher Scientific Themis Z microscope, equipped with a probe corrector, a four-segment DF4 detector, and a Gatan GIF Continuum dual-EELS system, combined with a new-generation K3 camera. STEM-EELS experiments were performed with a probe current of 30 pA and a collection angle of 100 mrad. Spectrum image (SI) data were acquired in Gatan GIF Continuum dual-EELS mode, with a spectrometer energy dispersion of 0.35 eV per channel. EELS maps were acquired with an exposure time of 0.03 s per pixel, and the acquisition conditions were consistent with those of the SI data acquisition.

Data availability

All data are available in the main text or supplementary information, and the original TEM and EELS data for this study can be accessed online at https://figshare.com/s/37d9b313416b8b2aaabc.

Received: 17 November 2025; Accepted: 15 January 2026;
Published online: 01 April 2026

References

1. Dibb, S. D. et al. A post-launch summary of the science of NASA's Psyche mission. *AGU Adv.* **5**, e2023AV001077 (2024).
2. Kargel, J. S. Metalliferous asteroids as potential sources of precious metals. *J. Geophys. Res. Planets* **99**, 21129–21141 (1994).
3. Grier, J. & Rivkin, A. S. *Airless bodies of the inner solar system: Understanding the process affecting rocky, airless surfaces*. (Elsevier, 2018).
4. Heiken, G., Vaniman, D. & French, B. M. *Lunar sourcebook: A user's guide to the Moon* (Cup Archive, 1991).
5. Lin, Y. et al. Return to the Moon: new perspectives on lunar exploration. *Sci. Bull.* **69**, 2136–2148 (2024).
6. Kullerud, G., Yund, R. & Moh, G. Phase relations in the Cu-Fe-S, Cu-Ni-S, and Fe-Ni-S systems. *Econ. Geol. Monogr.* **4**, 323–343 (1969).
7. Rubin, A. E. Metallic copper in ordinary chondrites. *Meteoritics* **29**, 93–98 (1994).
8. Tomkins, A. G. What metal-troilite textures can tell us about post-impact metamorphism in chondrite meteorites. *Meteorit. Planet. Sci.* **44**, 1133–1149 (2009).
9. Xie, X., Gu, X. & Yang, Y. The occurrence of metallic copper and redistribution of copper in the shocked Suizhou L6 chondrite. *Acta Geochim.* **43**, 827–837 (2024).
10. Łuszczek, K. & Krzesińska, A. M. Copper in ordinary chondrites: Proxies for resource potential of asteroids and constraints for minimum-invasive and economically efficient exploitation. *Planet. Space Sci.* **194**, 105092 (2020).
11. Burgess, K. D. & Stroud, R. M. Exogenous copper sulfide in returned asteroid Itokawa regolith grains are likely relicts of prior impacting body. *Commun. Earth Environ.* **2**, 115 (2021).
12. Carter, J. et al. Morphology and composition of chalcopyrite, chromite, Cu, Ni-Fe, pentlandite, and troilite in vugs of 76015 and 76215. In *Lunar Science Conference Proceedings* **6**, 719–728 (1975).
13. El Goresy, A., Ramdohr, P. & Taylor, L. A. The opaque minerals in the lunar rocks from Oceanus Procellarum. In *Proceedings of the Lunar Science Conference* **2**, 219–235 (1971).
14. Gornostaeva, T., Kartashov, P., Mokhov, A., Rybchuk, A. & Basilevsky, A. Natural alloys of the Cu–Ni system from impactites of the Lonar Crater (India) and Lunar Regolith. *Sol. Syst. Res.* **58**, 377–387 (2024).
15. Simpson, P. & Bowie, S. Quantitative optical and electron-probe studies of the opaque phases. *Science* **167**, 619–621 (1970).
16. Guo, Z. et al. Vapor-deposited digenite in Chang'e-5 lunar soil. *Sci. Bull.* **68**, 723–729 (2023).
17. Li, J. et al. First discovery of impact-induced vapor deposition of native copper, FeCo alloy and digenite from Chang'e-5 lunar soil. *Icarus* **415**, 116082 (2024).
18. Liu, X. et al. Sulfur isotopic fractionation of the youngest Chang'e-5 basalts: constraints on the magma degassing and geochemical features of the mantle source. *Geophys. Res. Lett.* **49**, e2022GL099922 (2022).
19. Taylor, L. A. & Williams, K. L. Cu-Fe-S phases in lunar rocks. *Am. Mineralogist: J. Earth Planet. Mater.* **58**, 952–954 (1973).
20. Cui, Z. et al. A sample of the Moon's far side retrieved by Chang'e-6 contains 2.83-billion-year-old basalt. *Science* **386**, 1395–1399 (2024).

21. Qian, Y. et al. Long-lasting farside volcanism in the Apollo basin: Chang'e-6 landing site. *Earth Planet. Sci. Lett.* **637**, 118737 (2024).
22. Yue, Z. et al. Geological context of the Changae-6 landing area and implications for sample analysis. *Innovation* **5**, 100663 (2024).
23. Zhang, Q. W. et al. Lunar farside volcanism 2.8 billion years ago from Chang'e-6 basalts. *Nature* **643**, 356–360 (2024).
24. Li, C. et al. Nature of the lunar far-side samples returned by the Chang'E-6 mission. *Natl. Sci. Rev.* **11**, nwae328 (2024).
25. Yang, J. et al. Complex impact processes on the Moon's farside recorded by Chang'e-6 low-Ti basalt. *npj Space Explor.* **1**, 10 (2025).
26. Cao, Z. et al. Submicroscopic magnetite may be ubiquitous in the lunar regolith of the high-Ti region. *Sci. Adv.* **10**, eadn2301 (2024).
27. Yan, P. et al. Submicroscopic iron-rich grains throughout impact glasses in Chang'E-5 regolith. *Icarus* **410**, 115920 (2024).
28. Mccoy, T. J., Dickinson, T. L. & Lofgren, G. E. Partial melting of the Indarch (EH4) meteorite: a textural, chemical, and phase relations view of melting and melt migration. *Meteoritics* **34**, 735–746 (1999).
29. Skinner, B. J. High crystallization temperatures indicated for igneous rocks from Tranquillity Base. *Science* **167**, 652–654 (1970).
30. Bennett, M. E. III & McSween, H. Y. Shock features in iron-nickel metal and troilite of L-group ordinary chondrites. *Meteorit. Planet. Sci.* **31**, 255–264 (1996).
31. Waldner, P. Energy modeling of high-temperature bornite: application on calculation of phase equilibria of the Cu-Fe-S system. *J. Phase Equilibria Diffus.* **46**, 170–185 (2025).
32. Waldner, P. The high-temperature Cu-Fe-S system: thermodynamic analysis and prediction of the liquid–solid phase range. *J. Phase Equilibria Diffus.* **43**, 495–510 (2022).
33. Li, C. et al. Vacuum-thermal alteration of lunar soil: Evidence from iron whiskers on troilite in Chang'e-5 samples. *Geochim. et. Cosmochim. Acta* **387**, 28–37 (2024).
34. Guo, Z. et al. Sub-microscopic magnetite and metallic iron particles formed by eutectic reaction in Chang'E-5 lunar soil. *Nat. Commun.* **13**, 7177 (2022).
35. Matsumoto, T., Harries, D., Langenhorst, F., Miyake, A. & Noguchi, T. Iron whiskers on asteroid Itokawa indicate sulfide destruction by space weathering. *Nat. Commun.* **11**, 1117 (2020).
36. Matsumoto, T. et al. Space weathering of iron sulfides in the lunar surface environment. *Geochim. et. Cosmochim. Acta* **299**, 69–84 (2021).
37. Thompson, M. S., Davidson, J., Schrader, D. L. & Zega, T. J. Sulfide minerals bear witness to impacts across the solar system. *Nat. Commun.* **16**, 5975 (2025).
38. Keller, L. P. & McKay, D. S. Discovery of vapor deposits in the lunar regolith. *Science* **261**, 1305–1307 (1993).
39. Pang, R. et al. Characteristics of space weathering modification of Chang'e-5 lunar soil: evidence from the microanalysis of anorthite. *J. Geophys. Res. Planets* **130**, e2024JE008611 (2025).
40. Pang, R. et al. Redox condition changes caused by impacts: insights from Chang'e-5 lunar glass beads. *Sci. Bull.* **69**, 1495–1505 (2024).
41. Anand, M. et al. Space weathering on airless planetary bodies: Clues from the lunar mineral hapkeite. *Proc. Natl. Acad. Sci. USA* **101**, 6847–6851 (2004).
42. Widom, E., Rubin, A. E. & Wasson, J. T. Composition and formation of metal nodules and veins in ordinary chondrites. *Geochim. et. Cosmochim. Acta* **50**, 1989–1995 (1986).
43. Yund, R. A. & Kullerud, G. Thermal stability of assemblages in the Cu—Fe—S system. *J. Petrol.* **7**, 454–488 (1966).

Acknowledgements

The authors are grateful to the China National Space Administration (CNSA) for providing the Chang'e-6 returned lunar samples. We acknowledge funding support from the Natural Science Foundation of China (grant number 42303039), RGC General Research Fund (17307025), and the Seed Fund for Basic Research for New Staff (2401102770).

Author contributions

Z.G. contributed to the conception, methodology, investigation, and paper writing of the paper. D.S. and W.S. contributed to the methodology and investigation. C.L. and R.P. contributed to the sample preparation. Yuqi Qian and K.H. contributed to methodology. Y.L. and G.Z. were responsible for the conception, paper revision, and funding acquisition.

Competing interests

The authors declare no competing interests.

Additional information

Supplementary information The online version contains supplementary material available at https://doi.org/10.1038/s44453-026-00027-y.

Correspondence and requests for materials should be addressed to Zhuang Guo or Yang Li.